Spring 5-31-2021

Isolation and Determination of the Composition and Structural Components that Comprise Dissolved Organic Matter Using Normal Phase Liquid Chromatography

Jonathan A. Long Jr
University of New Orleans, jalong3@uno.edu

Isolation and Determination of the Composition and Structural Components that Comprise Dissolved Organic Matter Using Normal Phase Liquid Chromatography

A Thesis

Submitted to the Graduate Faculty of the
University of New Orleans
in partial fulfillment of the
requirements for the degree of

Master of Science
in
Chemistry

By

Jonathan Allen Long Jr.

B.S. University of New Orleans, 2017

May 2021

ACKNOWLEDGEMENTS

I would like to begin by thanking my family for their continuous love and support throughout my graduate school experience. Specifically, I would like to thank my mother, Debra Long, and my aunt, Tracey Long.

This milestone in my life would not have been possible without the support I've received from my friends along the way. There are five people that I'd like to specifically acknowledge in this section, the first of which is Nichole Pianovich. We met in the spring of 2015, and as time went on, she went from being a stranger to someone that I consider to be family. The next person I'd like to acknowledge is Jason Hood. He's basically the brother I never had. Whether it be helping me with physics or showing me how to change a taillight, he always finds a way to help me when I need it. Sarah Gauthier is the next person I would like to recognize, and she's probably the most important of the five people. This is because her journey in grad school has already come to an end. This allows her to empathize with what I have going on. It also allows her to offer perspective, on what's going on so I can focus on the long term gain. Janelle Do is the last person I would like to acknowledge. Janelle helped me stay true to my processes and avoid taking shortcuts, always reminding me that shortcuts may get you to the end of the journey faster, but without all the memories and learning that comes with the traditional path.

I would like to thank both of my advisors, Dr. Zito and Dr. Podgorski, for their continuous support and guidance throughout my time in grad school. Lastly, I'd like to acknowledge the financial support from the Board of Regents (Reference #: 20130010705).

Table of Contents

List of Figures

* The corresponding file list for EEM's can be found in appendix.

List of Tables

List of Plots

Abstract

To study the reactivity of complex mixtures, understanding the different processes affiliated with them are key. A separation procedure was developed to obtain a complete representation of the aromatic subfraction of the light and heavy crude oil sample. The crude oils were separated into four fractions based on the number of condensed aromatic rings present. The dissolved organic matter (DOM) was generated from each fraction via thin films (30 μm) and a 12 h photodegradation time. DOM generated from each fraction was subjected to a photodegradation time series from 0 – 96 h in 24 h increments. Each DOM degradation series was measured using excitation emission matrix spectroscopy (EEMs) and statistical analysis were applied using parallel factor analysis (PARAFAC), to identify the underlying fluorophores present in the sample set. The 2% loading of sample provided the desired fractions. Dissolved organic carbon and absorbance measurements collectively decreased with increasing exposure time.

Keywords: Dissolved Organic Matter, Normal-Phase Liquid Chromatography, Parallel Factor Analysis, photodegradation

Introduction

Structural Complexity of DOM and the Carbon Cycle

The genesis of dissolved organic matter (DOM) can be linked to two overall sources, the first being terrestrial derived DOM and the second being marine derived DOM. Each giving rise to slightly different variations of generated DOM. Marine derived DOM is understood to come from the decay of phytoplankton and is believed to consist of 25-50% proteins, 5-25% lipids, and up to 40% carbohydrates.[9] While terrestrial derived DOM is the byproduct of biological degradation (i.e. biomass, plant litter, and soil organic matter) that reaches the ocean via rivers, lakes, and glaciers. Degradation of vascular plants yields DOM containing 10% proteins, 30-50% carbohydrates, some lipids found in the roots and leaf cuticles, 15-25% lignin, and other biomacromolecules.[9-12]

Of the byproducts formed, carbohydrates and proteins are considered to be biolabile due to the nature of their chemical structure. This is due to their susceptibility to hydrolysis at the hands of different enzymes present in the environment. The hydrolysis reaction takes place at the areas where peptide and glycosidic bonds are located.[9] Lignin, on the other hand, exists as a branched macromolecular system, comprised of repeating phenylpropanoid units, which are connected by ether and carbon-carbon bonds at differing locations throughout the structure (Figure 2). This structural design supports the chemical stability of lignin, which results in a chemical resistance to microbial degradation.[9]

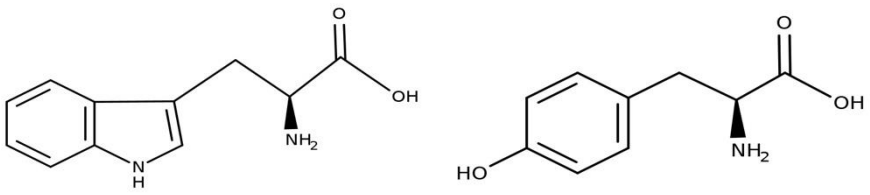

Figure 1. Chemical structure of tryptophan (left) and tyrosine (right) amino acids.

As DOM is photodegraded, a cascade effect begins to take place that inevitably ends when the starting compounds reach a point where they cannot be reduced anymore. When compounds

cannot be reduced, one of a few classifications can remain: tyrosine-like, tryptophan-like, humic-like, or fulvic-like (Figure 1).

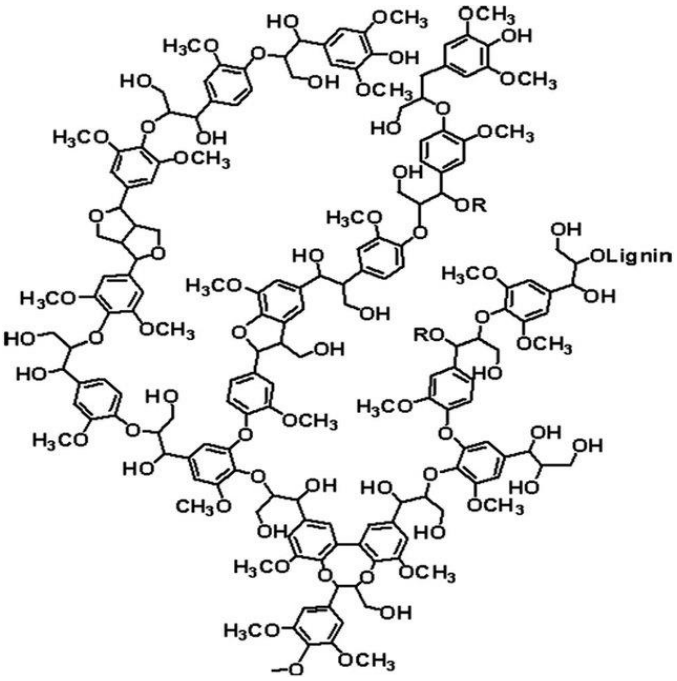

Figure 2. A structural depiction of one of the chemical byproducts of vascular plant decay known as lignin[1]. Reprinted with permission from Prieur, B., et al., *Phosphorylation of lignin: characterization and investigation of the thermal decomposition.* RSC Adv., 2017. **7**: p. 16866-16877. Copyright 2017 by The Royal Society of Chemistry.

Understanding the complex organic components that comprise DOM has become the primary focus of many studies over the recent years. Figure 2, illustrates a traceable structure affiliated with DOM, known as lignin, due to its resistance to degradation processes in the global carbon cycle. A detailed understanding of the molecular structures and associated reactivities of specific classes of molecules that are present in the complex mixture of DOM can allow for inferences to be made regarding how they will be broken down and subsequently cycled. Figure 3 shows the different pathways by which dissolves organic carbon (DOC) is cycled.

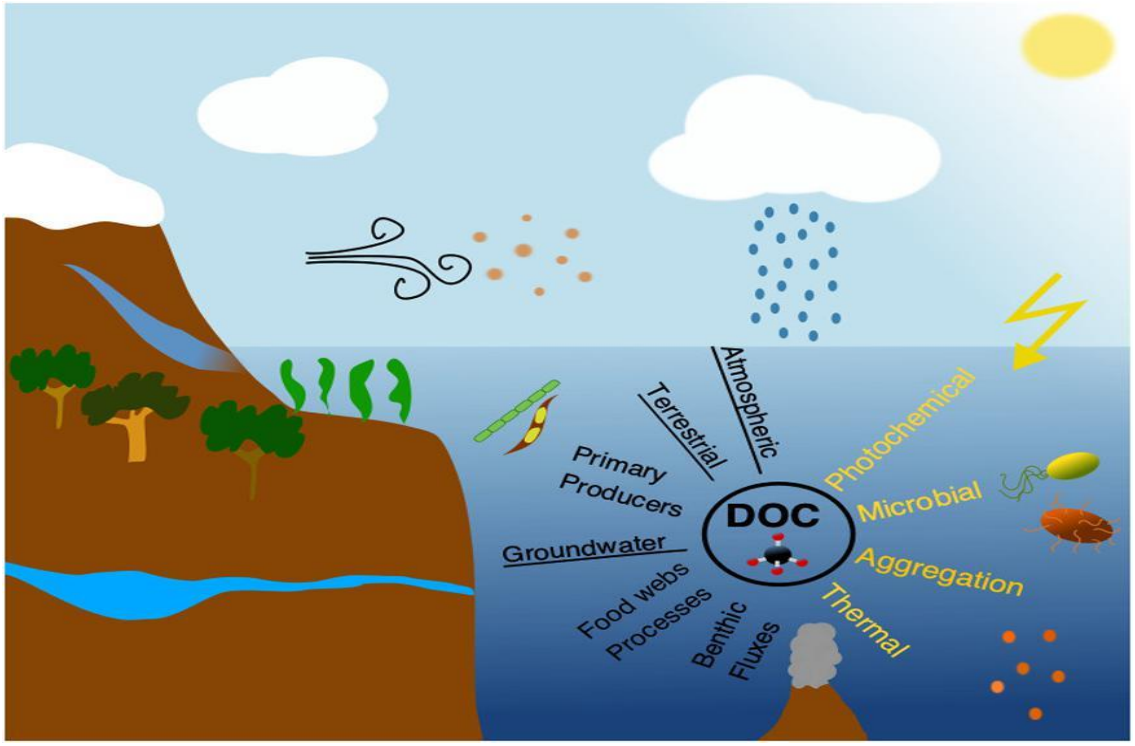

Figure 3. To the left the main input sources can be seen (black) and to the right the degradation are degradation (DOC removal) pathways (yellow).[13]

Insights into the structures that comprise this complex mixture can provide vital information that will inevitably help to develop an understanding of their reactivities by various degradation pathways.[6, 13-18] Photochemical degradation of DOM molecules found in surface waters have already been found to considerably affect the composition and quantity of dissolved organic carbon (DOC) carried through marine systems[19].

Composition of Crude Oil

Crude oil is comprised of hundreds of different hydrocarbons and other organic and inorganic substances including sulfur, nitrogen, and oxygen, as well as metals like vanadium and nickel.[20] The percent abundance for the different elements found in petroleum are shown in table 1.

Elemental Analysis	Light Crude (wt %)	Heavy Crude (wt %)
Carbon	86.0	87.0
Hydrogen	13.5	10
Nitrogen	0.2	0.3-0.5
Oxygen	<0.5	<0.1
Sulfur	<2.0	3.0
Nickel (ppm)	<10.0	16
Vanadium (ppm)	<10.0	50

Table 1. Weight percentage for carbon, hydrogen, nitrogen, oxygen, sulfur, nickel, and vanadium.[4, 21]

Variations in the amount of each element present gives rise to crude oils that differ in physical properties. The two types of oil used in this study are Macondo surrogate oil (MC252) and Maya sour crude oil. The properties of the two oils are detailed in Table 3. Macondo surrogate oil has an API gravity of 37.2, a low viscosity, and is classified as light oil. Whereas the Maya crude oil has an API gravity of 22.2, a highly viscous oil, and is classified as a heavy oil. Light oil contains a low concentration of heteroatoms. This can be seen by the low weight percent for nitrogen, oxygen, sulfur, nickel, and vanadium displayed in table 1. In contrast, heavy oils possess higher concentrations of heteroatoms, which is supported by the higher weight percentages found for nitrogen, oxygen, and sulfur in table 1.

Aspect	**Macondo**	**Maya**
API°	37.2	22.2
Specific Gravity	0.839	0.922
Density (g/cm^3)	0.839	0.921
Viscosity	Low	High
Classification	Light	Heavy

Table 2. Comparison of the characteristics exhibited by Macondo surrogate oil and Maya sour crude oil.[4]

A mixture of a heavy and light oil was used to obtain a full distribution of compounds that adequately represent the structural continuum. This is necessary because, at the molecular level, the variations found between the light and heavy oil, complement one another. The light oil

provides saturated, as well as, mono and dicyclic compounds. Heavy oil possesses the larger aromatic systems needed to represent the structural continuum (Figure 4).

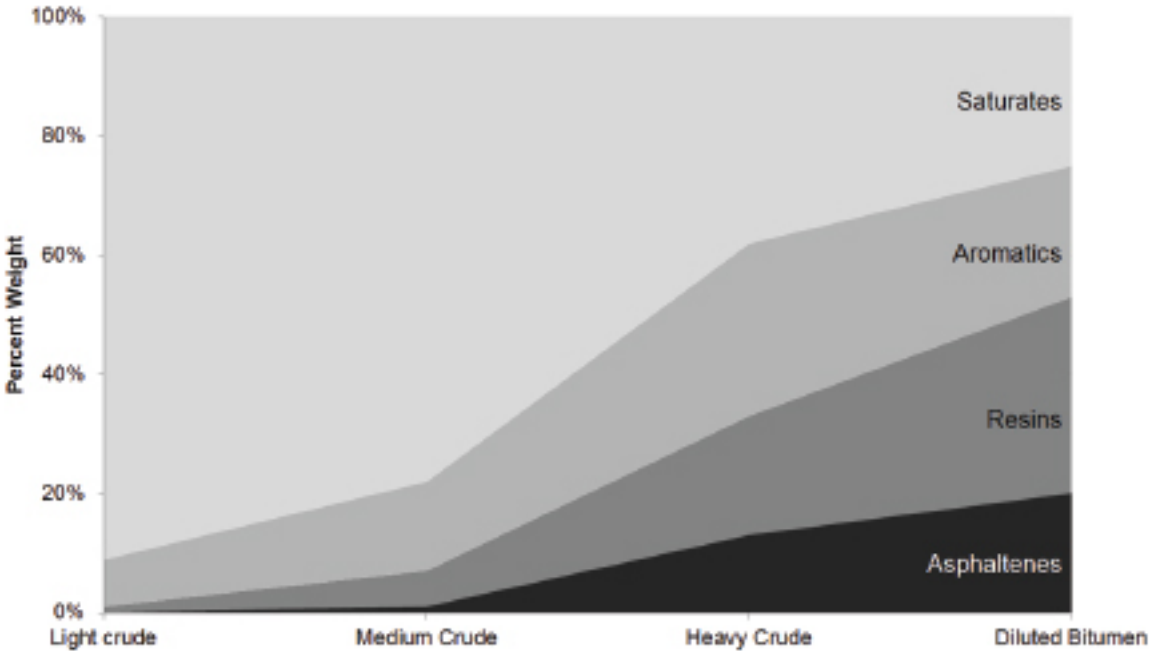

Figure 4. The distribution of weight percentages of typical components found in light, medium, and heavy crude oil's[2]. Reprinted in part with permission from Environment, C.; Technology, B.; Studies, D.; Medicine, N., *Spills of diluted bitumen from pipelines: A comparative study of environmental fate, effects, and response*. 2016; p 1-166. Copyright 2016 by the National Academy of Sciences.

Asphaltenes are the portion of crude oil that are insoluble in alkanes, such as n-heptane and n-pentane, and are defined by their solubility characteristics in place of a specific chemical characterization.[5, 22-24] Given their unique composition, heteroatoms are able to influence surrounding asphaltene compounds into sticking together by playing off the polarizability of the aromatic systems that are locked into configuration in combination with subtle variations in charge separation.[22] Light oils has lower concentrations of asphaltenes than heavy oils. Oils that contain higher concentrations of asphaltenes are darker in color and exhibit a higher viscosity than that of oils with lower concentrations of asphaltenes.[22] The chemical composition of the Maya crude oil used in this study is classified as a heavy oil, and as such, is prone to having higher concentrations of asphaltenes than the Macondo surrogate oil.

The structure of asphaltenes can vary in type which can influence their properties. An example of an archipelago style asphaltene can be seen on the left in Figure 5. It is comprised of two condensed aromatic cores that are linked together by an aliphatic chain. Another style of asphaltene is the island configuration which is comprised of a single condensed aromatic core with aliphatic chains branching from outside rings.[3] Asphaltenes, regardless of the structural orientation, are described as being insoluble in excess solvents made of nonpolar compounds (i.e. pentane and heptane).[25]

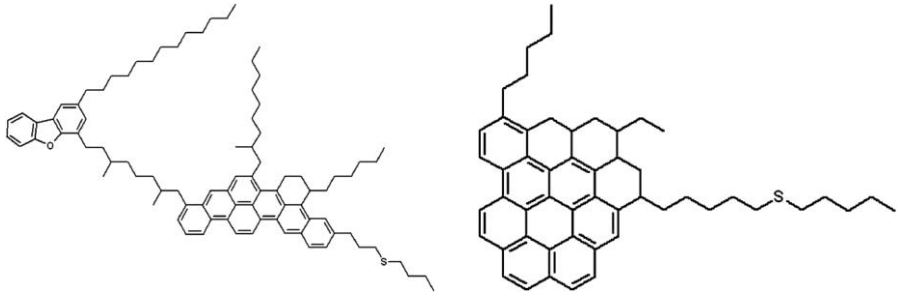

Figure 5. Two examples of asphaltene chemical structures. On the left, an example of an archipelago type asphaltene. On the right, an example of an island type asphaltene[3]. Reprinted in part with permission from Boek, E., T. Headen, and J. Padding, *Multi-scale simulation of asphaltene aggregation and deposition in capillary flow*. Faraday discussions, 2010. **144**: p. 271-84; discussion 323. Copyright 2010 by Faraday Discussions.

Once the asphaltenes are precipitated out of solution, the remaining product is comprised of what is described as 'maltenes'. The maltenes fraction of crude oil is made up of saturated, aromatic, and resin like compounds.[5, 26] Humic acids vary in structure depending on the source material from which it is derived. In comparison with fulvic acids, humic acids are larger have a lower oxygen content and a low solubility in water at neutral pH. The lack of solubility can be attributed to the lack of oxygen in the structure. In contrast, fulvic acids have a much higher oxygen content and dissolve more rapidly in water.

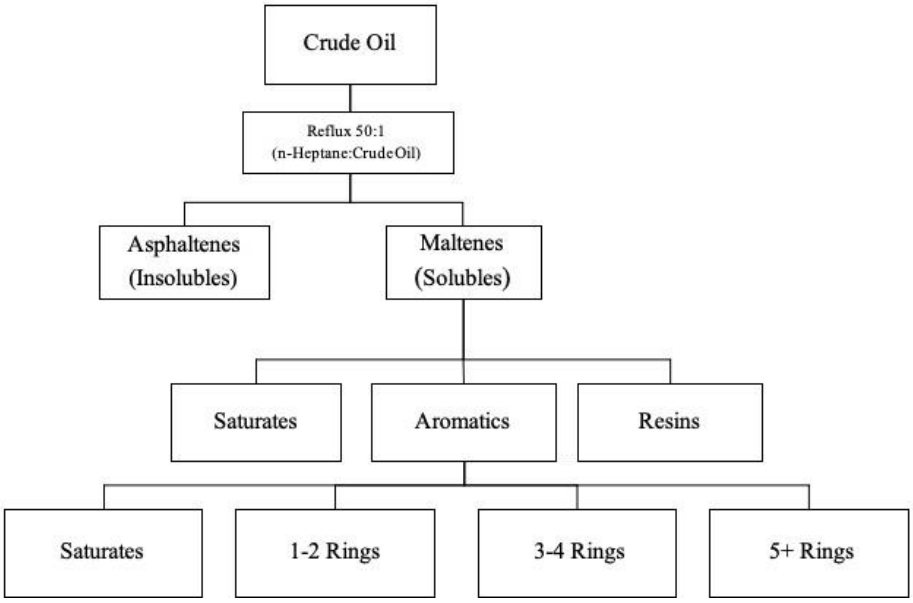

Figure 6. SARA fractionation of crude oil with subsequent fractionation of the 'aromatic' division into discrete bins based on the number of rings[4, 5]. Adapted with permission from Gaspar, A., et al., *Characterization of Saturates, Aromatics, Resins, and Asphaltenes Heavy Crude Oil Fractions by Atmospheric Pressure Laser Ionization Fourier Transform Ion Cyclotron Resonance Mass Spectrometry.* Energy & Fuels, 2012. **26**(6): p. 3481-3487. Copyright 2012 by the American Chemical Society.

Sub fractionation of the aromatic portion of maltenes and Macondo surrogate oil mixture provides insight into the underlying components that gave rise to the features that define the overall sample. In order to understand the whole picture, each individual fraction possesses a unique characteristic that plays a role in the final answer. From the separated aromatic rings, photo exposure experiments can be performed to introduce oxygen atoms into the separated ring fractions to resemble compounds found in aquatic environments. This will lead to insight into identifying which core structural bins these different compounds originate from. This can be achieved because specific fluorophores are defined by specific excitation and emission wavelengths.[27]

Boduszynski Continuum Model

Mieczyslaw Boduszynski published a series of articles that focused on the composition of heavy petroleum.[6, 28, 29]The first publication in the series explores variations in molecular weight, hydrogen deficiency, and heteroatom concentrations in response to the atmospheric equivalent boiling point (AEBP).[30] The data obtained shows that heavy petroleum, and its residues, are not comprised of predominately high molecular weight components. But rather, contain a distribution of molecular weights, with the highest molecular weight observed not exceeding 2000[30]. It was

also concluded that with an increase of AEBP the concentration of heteroatoms and hydrogen deficiency were seen to increase.[30]

The next publication in the series looks at molecular characterization utilizing two different methods[31]. The data obtained from the first method demonstrated changes in the concentrations of the molecular building blocks as AEBP increases and solubility decreases.[30, 31] The second method centers on utilizing high-performance liquid chromatography (HPLC) to separate compound class fractions for more in-depth molecular characterization.[31] Results obtained from the second method showed a diversity of molecular types, with multiple homologous series of compounds, each series having a broad carbon distribution.[31]

Boduszynski and his team also completed a separation of 50 polycyclic aromatic hydrocarbons (PAH) using an amino functionalized silica stationary phase[6]. This allowed the PAH compounds to elute based on the number of aromatic rings. By separating the PAHs based on their core ring structure, the method could potentially be applied to a more complex sample, such as the maltenes fraction of crude oil. Separating the maltenes based on their core ring structure would provide a way to reduce the complexity of the sample by yielding different subclasses that could be studied individually.

Normal-Phase Liquid Chromatography (NPLC)

The properties and behavior exhibited by crude oil can be better understood by developing a fundamental understanding of the different chemical components that comprise it.[26, 32] To obtain a better understanding the SARA (Saturates, Asphaltenes, Resins, and Aromatics) fractionation procedure is frequently used to separate crude oil samples into their underlying constituents.[5, 33] In Figure 8 illustrates the procedure for how the SARA method fractionates crude oil into its underlying components on the basis of each fractions solubility. For this study, the aromatic fraction was chromatographically separated in a second dimension by number of aromatic rings. of the aromatics based on the number of rings, DOM was generated by photochemical oxidation of the residues that corresponded to each fraction.

The complex mixture can be separated into different classes, which will be comprised of compounds that share similar structural characteristics, by employing normal phase liquid chromatography (NPLC).[6, 34, 35] This process can be achieved because of the differences in structure, and subsequently the polarity, exhibited by each of the fractions. The differences will allow the fractions to interact with the stationary phase at different strengths to increase the quality

of the separation. The stationary phase used in this study was 3-aminopropyl functionalized silica gel and is shown in Figure 7 below.

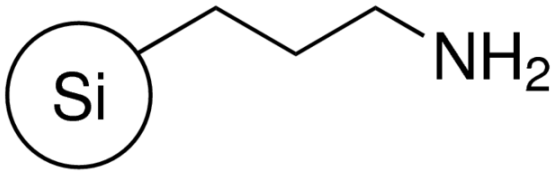

Figure 7. Structural depiction for 3-aminopropyl silica functionality used in the chromatographic separation.

The elution will yield the saturates fraction first, since they are the least polar and will interact the least with the more polar stationary phase. To get the more polar fractions to elute, alterations to the mobile phase will have to be made by adding a more polar solvent to the mobile phase to mitigate the interactions occurring between them and the stationary phase.

Boduszynski and his team found that by using functionalized silica the mixture could be separated into different classes based on the number of aromatic rings found in the sample.[6] In Figure 8, the results obtained by Boduszynski et al. (1983) for the separation of heavy oil at the analytical level can be seen.

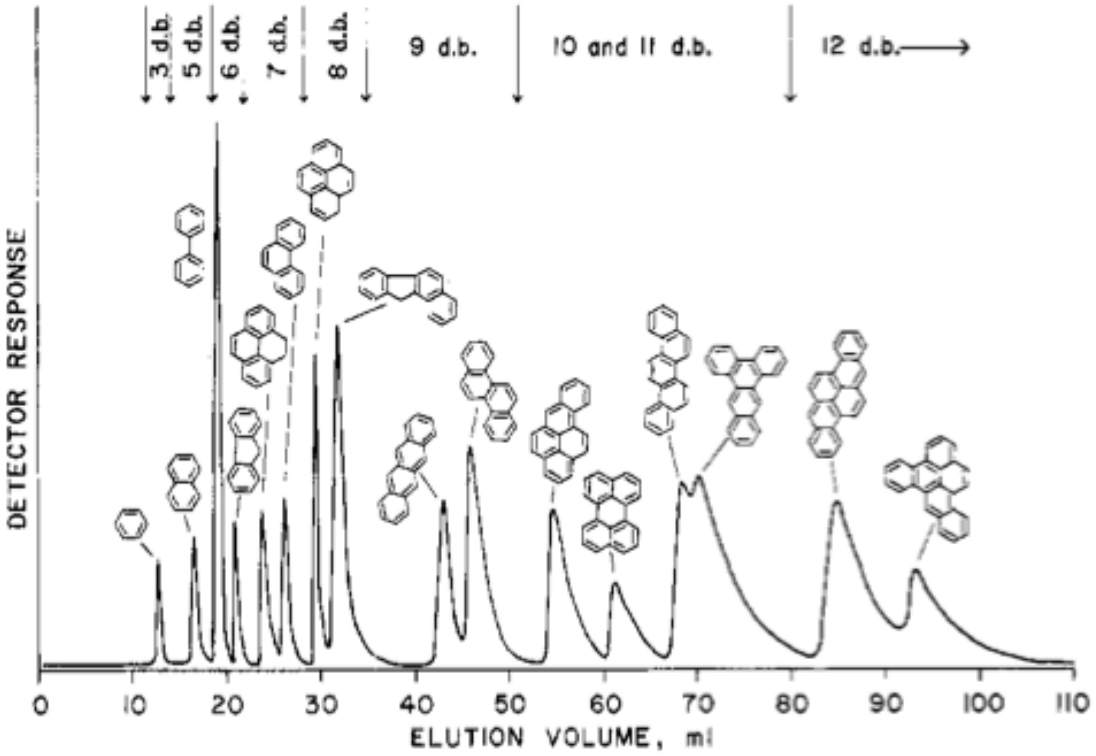

Figure 8. Elution profiles of Polyaromatic Hydrocarbons (PAH) on a semiprepartive μBondpak NH_2 Column[6]. Adapted with permission from Boduszynski, M. M.; Hurtubise, R. J.; Allen, T. W.; Silver, H. F., Liquid-Chromatography Field-Ionization Mass-Spectrometry in the Analysis of High-Boiling and Nondistillable Coal Liquids for Hydrocarbons. *Analytical Chemistry* **1983,** *55* (2), 225-231. Copyright 1983 American Chemical Society.

The use of 3-Aminopropyl functionalized silica provided the necessary means to separate the mixture based on the number of rings present, with adequate selectivity and resolution.[17, 36, 37] Preparative chromatography was used to scale up the separation procedure so that enough of each ring fraction could be obtained to make a 30 μm oil film for the DOM generation section of the study. Upon scaling up the reaction, issues began to arise with maintaining reproducibility with respect to the column volume which affected the integrity of the separation. As a result, it can be seen how to appropriately account for intersitial volume between particles as well as pore size (Figure 9).

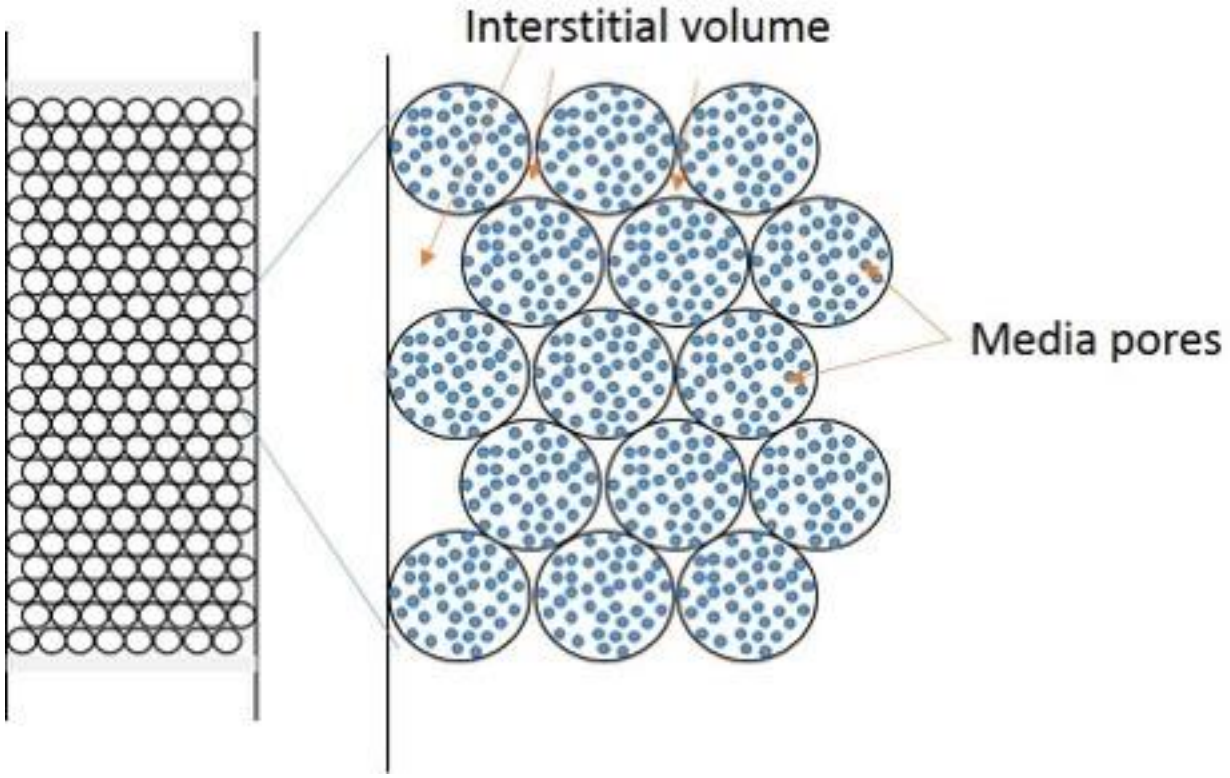

Figure 9. Visualization of intersititial and pore volume in relation to column volume.[7, 8]

For the purpose of this study, a combination of Macondo surrogate oil and Maya Sour Crude oil were combined to makeup the sample (Table 2). This was to provide a sufficient balance of low molecular weight compounds with high molecular weight compounds.

Removal of Carbon via Photochemical Pathways

The degradation of DOM involves a complex overlay of different disciplines including biological, chemical, and photochemical pathways.[38] Photochemical removal is important when considering the fate of DOM because it yields products that are then exposed to microbial degradation.[38] The production of oxygenated compounds as a function of time in the presence of sunlight has been proven to occur when petroleum is exposed to water.[39-41] Upon photooxidation, compounds that started off being oil soluble are now closer to being water soluble.[39] To elucidate the pathways by which these newly water soluble compounds are transported, the ring specific fractions collected from the separation described in the previous section were used to produce aromatic DOM.[39]

Parallel Factor Analysis (PARAFAC)

Advancements in spectroscopic instrumentation (i.e. absorbance and fluorescence) and data processing programs have yielded a rapid and highly sensitive way to extract information from samples to help in the characterization of DOM.[39, 42] Parallel factor analysis (PARAFAC) is a multivariate modeling statistical analyses which highlights the underlying fluorescent components of the sum of 40 spectra reducing them to four specific components. .[25, 43]

The first step in obtaining any PARAFAC model begins with preprocessing the data set being used. This preprocessing step is to adjust for any biases, remove any scattering that may be present, and to normalize the data. Normalizing the signals of all samples is crucial because it allows all samples in the dataset, regardless of high or low concentration, similar weight. This allows the generated PARAFAC model to focus, not on the intensity of all the signals in the set, but rather the chemical variations exhibited between the samples.[44]

Next, multiple exploratory phases will be completed to develop potential models in order to locate and remove any outliers present in the sample set. In this exploratory phase it will be key to identify the correct number of components, such that there is significant distribution of variation across the data, resulting in a model that only encompasses random errors.[44] The model that yields the highest core consistency at the end of the exploratory phase will indicate the appropriate number of components to be used to represent the model as a whole.[44, 45]

The final step in the PARAFAC process is the model validation step and its success is heavily reliant on using the appropriate number of components when fitting the model.[44] Under or overcompensating the number of components in the dataset, when attempting to validate the method, will prevent the model from validating. When a model is fitted with an insufficient number of components, the validation failure occurs as a result of the model erroneously grouping signals that are representative of components that are distinctly different. Attempting to validate a model using too many components will fail due to an overlap of multiple components in the dataset, resulting in the model mistakenly coupling multiple PARAFAC moieties as one component.[44]

Once the PARAFAC model is completed, the model can be uploaded to OpenFluor, an online repository containing already published fluorescence spectra, to identify similar spectra so that more information can be extracted from the model.

Experimental Methods

Asphaltene Precipitation

Maya sour crude oil and n-heptane were added to a 1000 mL round bottom flask in a ratio of 1:50. The mixture was then heated and refluxed at a temperature of 100 °C for 1 hour. After 1 hour, the solution was removed from the heat and allowed to continue refluxing for 30 minutes and then was capped and stored overnight. The solution was then filtered through a Whatman #1 filter (11 μm) to isolate the maltenes fraction of the crude oil.

Column Packing and Separation Parameters

Contents	Fraction	Column Volumes	Solvent
Saturates	1	1	n-Heptane
1-2 Rings	2	1	n-Heptane
3-4 Rings	3	3	n-Heptane
5 Rings	4	2	2% Dichloromethane in n-Heptane
5+ Rings	5	2	10% Dichloromethane in n-Heptane

Table 3. Separation Parameters for Crude Oil Mixture.

Maltenes and MC252 Sample Preparation

Maltenes and MC252 oil were added to a vial in a 2:1 ratio respectively. The total mass of the sample was kept at a 2 % sample load with respect to the amount of stationary phase.

Photodegradation Time Series

Using the solar simulator (Atlas Suntest CPS+, Atlas Material testing Technology LLC) set at 765 W/m^2 one 24 hour interval is equivalent to four days of natural sun-light in the Gulf of Mexico[18]. Films were produced using each ring fraction obtained in Section 2.2. For a 30 μm film thickness, 87 mg of each respective fraction is required. To provide a uniform film 87 mg of sample was dissolved into 10 mL of n-heptane and 2 mL was poured over 50 mL of nanopure water inside a 250 mL jacketed beaker thermostatically controlled at 27^{o}C. Generation of DOM from each ring fraction was subjected to simulated sunlight for 24 hours. The DOM from each subsequent ring fraction (30 mL) was photodegraded from 0 to 96 hours in 24 hour increments. Quartz lids securely placed over the jacketed beakers to reduce evaporation yet still allow sufficient light through during all simulations.

562 ***Total Organic Carbon Analysis***

563 DOC concentrations were obtained via the Shimadzu total organic carbon (TOC) analyzer
564 using a high-temperature combustion method and a platinized alumina catalyst. A ratio of 1:3 (v/v)
565 was used to dilute the sample in nanopure water that was then acidified to a pH of 2 utilizing 12
566 M HCl. Samples were then sparged for 5 min at 75 mL/min with ultra high purity air to remove
567 the inorganic carbon from the samples prior to analysis. A five-point calibration curve was used
568 to determine the samples concentration utilizing a range from 0 to 50 ppm using potassium
569 hydrogen phthalate (KHP). To ensure the efficiency of the instrument, calibration curves ranging
570 from 0 to 50 ppm were conducted every 10 samples as well as at the end of the run. A 5 ppm check
571 was also integrated into the sample analysis to confirm maximum instrument efficiency. Blank
572 samples were run before and after all checks and calibration curves. To determine the DOC
573 concentration present in the sample, the best 3 injections of 5 were used to determine the DOC
574 present in a sample at an injection volume of 150 µL. The best 3 injections obtained should result
575 in a coefficient of variance of <2% for duplicate injections[39].

576 ***Absorbance Analysis***

577 All samples in the study were measured on an Agilent UV-Vis absorbance instrument, from
578 200 to 600 nm. Absorbance values corresponding to 254 nm were used for the specific UV-
579 absorbance ($SUVA_{254}$) calculation in conjunction with DOC values[27].

580 ***Fluorescence Analysis***

581 Excitation emission matrix spectroscopy (EEMs) measurements were collected at an
582 excitation range from 240 to 800 nm and emission from 240 to 800 nm using a 10 mm quartz
583 cuvette. Excitation spectra were collected every 5 nm and emission every 3 nm at a 1.5 second
584 integration time. Sample intensities were normalized to Raman scattering units (RSU) and
585 statistical analysis were applied using PARAFAC analysis. Inner-filter effects were mitigated by
586 correcting to 0.1, based on the absorbance value found at 254 nm, using nanopure water.[18, 46, 47]
587 The drEEM toolbox was utilized to produce a validated model, to yield a four component
588 PARAFAC model from 40 samples.[25, 44, 48]

589

Results and Discussion

Determination of Load Capacity

Loadings of 5, 10, and 20 mg were applied to HF-Mega BE-NH_2 solid phase extraction (SPE) cartridges to identify the optimal loading capacity. Based on the EEMs shown in Figure 10 below, it was determined that a 2 % loading of sample to stationary phase was optimal.

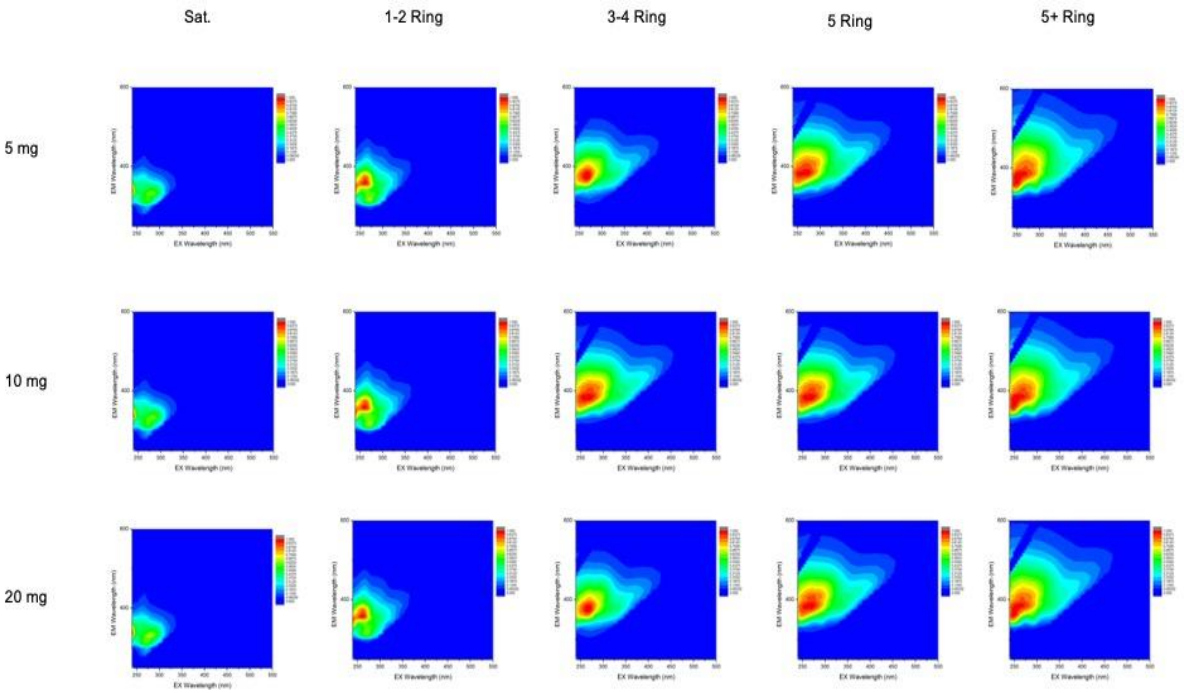

Figure 10. Fluorescence spectra confirming the 2 % loading had minimal carryover for each fraction.

The saturate fraction of oil is known to possess compounds that are aliphatic and alicyclic in structure.[5] Therefore, the EEMs taken for the saturate fraction should have a very small, if any, fluorescent signature. The signatures seen in Figure 10 for the saturate fraction were determined to be the 1 - 2 ring fraction that eluted earlier than anticipated. This occurred as a result of a miscalculation for the total column volume. This error was adjusted before the preliminary scale up was conducted.

Preliminary Scale Up

Before the final scale up, a preliminary scale up was completed to ensure that the separation could be sufficiently reproduced without losing quality. In Figure 11 below, a comparison of the

scaled down model at 1 gram of functionalized silica alongside the preliminary scale up at 20 grams of functionalized silica can be seen. The EEMs shown demonstrate that there is minimal loss of quality upon scaling up. After adjusting the column volume, the EEMs of the saturates fraction in the preliminary scale up reflects no coelution between the saturates and 1 - 2 ring fractions.

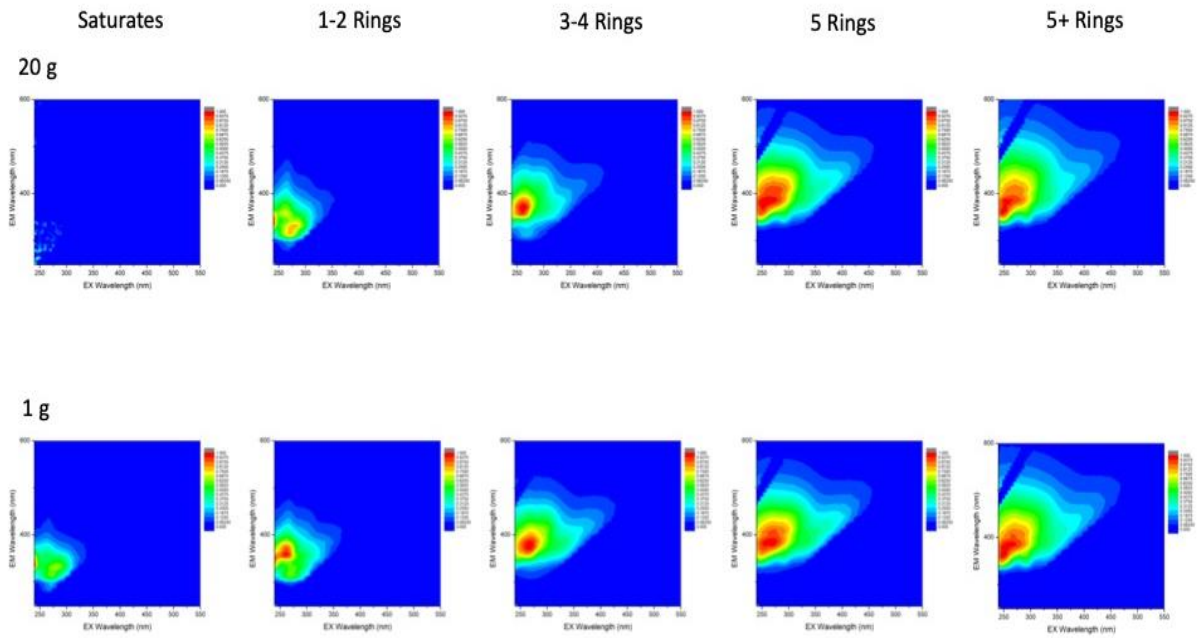

Figure 11. Comparison of scaled down EEMs with preliminary scale up EEMs for 20 g (top) and 1 g (below).

The alterations made to the column volume between the scaled down separation and the preliminary scale up returned results that accurately depict what is expected with respect to chemical theory, as well as supports the findings of previously completed studies that examined the chemical composition of the subfractions that makeup oil. As a result of their structural nature, compounds eluted within the 'saturates' fraction lack the conjugated π bond system necessary to yield a fluorescent signature. The lack of fluorescent signature found for the saturate fraction of the preliminary scale up depicted in Figure 11, displays some small sporadic signatures, but isn't representative of any specific moiety. For the preliminary scale up the EEM representing the saturate fraction of the separation possess some nondistinctive signatures that are shifted to the shortest wavelengths. Figure 11 shows that as the number of rings increase, the EEM's become

shifted to longer wavelength. EEMs collected for the 5 - ring and 5+ ring fractions displayed contour plots showing little difference between the two, therefore they were combined to represent the 5 + ring fraction.

Photodegradation of Fractionated Aromatic Ring Fractions

The adjustment to the column volume previously described previously, allowed for the subsequent final scale up, using the verified ratios between then preliminary scale up and the scaled down studies. The next portion of the study explores how these different fractions individual breakdown in the presence of sunlight. It can be seen in Plot 1 below, the general trend described by previous studies, that as exposure time increases the ratio of hydrogen to carbon (H/C) decreases and the ratio of oxygen to carbon (O/C) increases as oxygenation increases as a function of time.

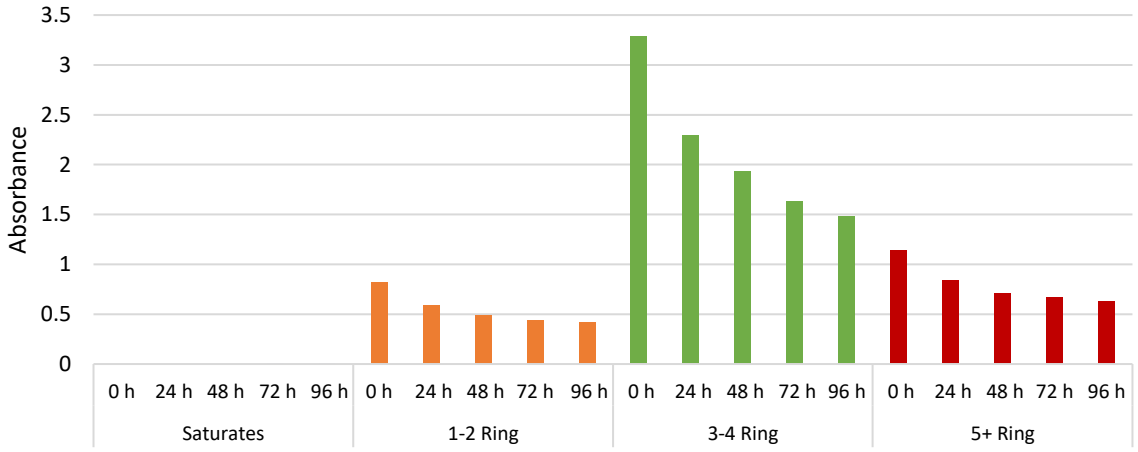

Plot 1. Absorbance values illustrating 1 - 2 ring DOM (orange), 3 - 4 ring (green) and 5 + ring (red) photodegradation time series.

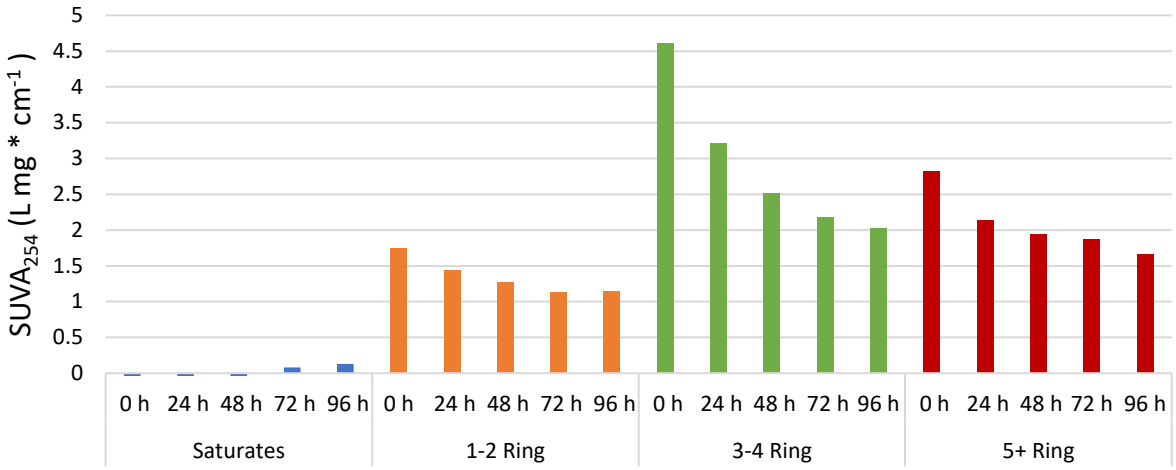

Plot 2. $SUVA_{254}$ (L mg * C^{-1} m^{-1}) for saturates (blue), 1 - 2 ring (orange), 3 - 4 ring (green) and 5+ ring (red). A decrease in $SUVA_{254}$ is observed as the photodegradation time is increased.

The application of $SUVA_{254}$ can be used as a proxy for the aromatic content in DOM.[49, 50] In Plot 2, it can be seen for all ring fractions, a decrease in aromaticity occurs with increasing exposure times.

PARAFAC Analysis

The EEMs for the photodegraded ring fractions were processed in MATLAB to remove outliers, excise and smooth the scatter regions, and to normalize to unit variance (Figure 12). The saturates timeseries displays no fluorescent signature due to the lack of conjugated double bonds. As a result, they are omitted from the PARAFAC process as outliers, because it will introduce additional variance into the model. After removal, a model can be constructed that better explains the differences between the degradation products that makeup the remaining samples.

For each fraction, the contour plot should decrease in intensity at its core and as stretch around the edges as the condensed aromatic rings begin to break and yield smaller compounds. This results as a byproduct of photooxidation. The smaller compounds will begin to introduce oxygen containing functionalities such as carboxylic acids, ketones, and aldehydes. A good representation of this trend can be seen for the 3 - 4 ring degradation series. In the 0 hour timepoint (Figure 12 - 4), a high intensity yellow core can be seen with surrounding regions that vary in shape and distance from the epicenter. The 24 hour timepoint (Figure 12 - 9), the concentric rings begin to gradually shift out as photooxidation occurs. This trend occurs throughout the remaining timepoints, and when the ninety-six hour time point is reached (Figure 12 - 15), the original

epicenter is now reduced to a small, less intense region with the outside bands stretching towards longer excitation wavelengths.

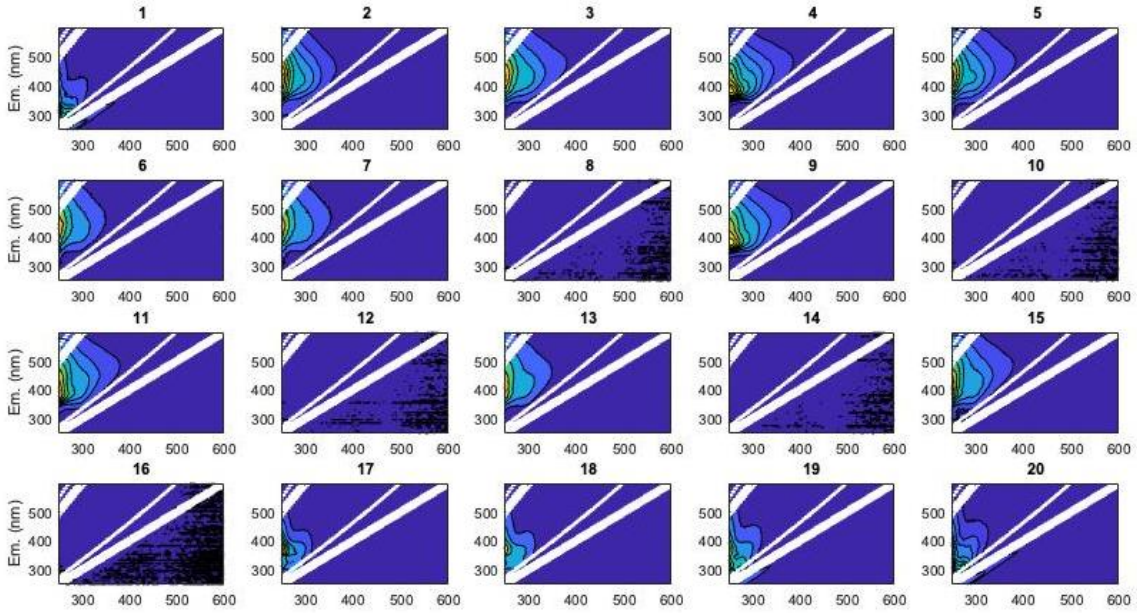

Figure 12. Corrected excitation emission scans of the photodegraded ring fractions.[†]

The validated PARAFAC model (Figure 13) portrays the fluorescent signatures that were present in all 40 samples. The model output was uploaded into OpenFluor, to identify similar components from other studies, to aid in building a more complete picture of the data that is present. Based on the fractions expected, an increase in emission is to be expected as the number of core aromatic rings per fraction increases. Any overlap in fractions can initially be attributed to overlap of the desired fractions.

[†] The corresponding file list for EEMs can be found in appendix.

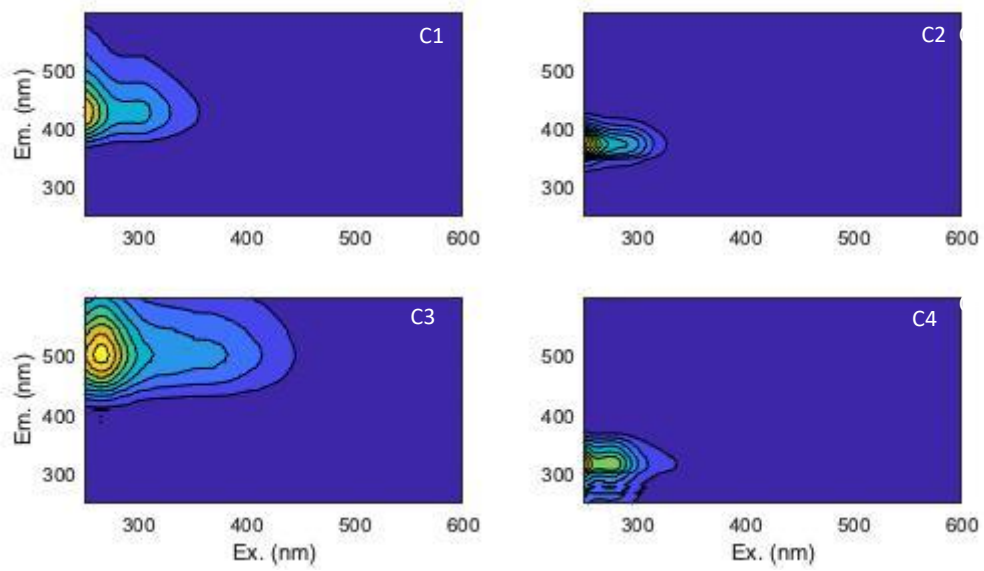

Figure 13. Validated 4 component model (C1 – C4) from the PARAFAC analysis.

A four component PARAFAC model was validated (Figure 13) showing a shift in excitation/emission wavelengths from shorter to longer wavelengths from C4, C2, C1 and C4, respectively. The first component, C1, (Figure 13) shows a initial excitation at 250 nm and then a secondary excitation at 305 nm, resulting in an emission maximum at 427 nm. This peak is found in a region characterized as marine humic-like in nature and is most likely derived from the 5 + ring fraction.[51, 52] This region can also be described as Peak A and is representative of blue shifted aromatic compounds that have a high molecular weight.[52]

Component 2 reflects characteristics described as protein-like and/or amino acid-like in nature.[53] Component 2 (C2) has a primary excitation at 250 nm and a secondary excitation at 290 nm, that result in an emission of 373 nm. With respect to C1, C2 is slightly more blue shifted and as a result is characteristic of the 3 - 4 ring fraction degradation products. The compounds present can be described as possessing low molecular weight and are high in aromaticity.[52]

Component 3 (C3) displayed a primary and secondary excitation at 265 nm and 370 nm, respectively. This resulted in an emission of 501 nm that can be related to the 5 + ring fraction. Despite the 5 ring and 5 + ring fractions being combined upon scale up, the PARAFAC model depicted these two fractions as two distinctly different components within the model. Since the C3 exhibited the longest excitation/emission wavelengths of all the components in this model, it can be inferred that it is representative of the 5 + ring fraction in the separation. Component 3

demonstrates a chlorophyll like terrestrial dominance in regard to chemical structure, which corroborates its affiliation with the 5+ ring fraction.[54]

Component 4 (C4) is the most blue-shifted of all the components, and as a result is considered to be best representative of the 1 - 2 ring fraction degradation products. The peak for this component can be described as mixture of tryptophan and tyrosine-type compounds, that resemble a protein like confirmation.[55] C4 also displays characteristics of photobleaching, which corroborates the nature of the component in terms of the model as a whole.[56]At this point in the photo degradation process, when the compounds yield a 'protein-like' structure, they tend to be less photolabile than that of humic substances.[56]

Conclusion

Utilizing a 2 % sample loading, with respect to the mass of the stationary phase, a uniform scale up was achieved with minimal overlap of the fractions desired. The error encountered during the scale up, using an open column separation approach, was identified to be the column volume used to define each respective fraction. When the components obtained from the validated model are rearranged, a linear relationship appears that represents the four separated fractions. The final component is indicative of compounds that are less likely, if not completely, exempt to photolability.

References

1. Prieur, B.; Meub, M.; Wittemann, M.; Klein, R.; Bellayer, S.; Fontaine, G.; Bourbigot, S., Phosphorylation of lignin: characterization and investigation of the thermal decomposition. *RSC Adv.* **2017,** *7*, 16866-16877.
2. Environment, C.; Technology, B.; Studies, D.; Medicine, N., *Spills of diluted bitumen from pipelines: A comparative study of environmental fate, effects, and response*. 2016; p 1-166.
3. Boek, E.; Headen, T.; Padding, J., Multi-scale simulation of asphaltene aggregation and deposition in capillary flow. *Faraday discussions* **2010,** *144*, 271-84; discussion 323.
4. Goual, L., Petroleum Asphaltenes. 2012.
5. Gaspar, A.; Zellermann, E.; Lababidi, S.; Reece, J.; Schrader, W., Characterization of Saturates, Aromatics, Resins, and Asphaltenes Heavy Crude Oil Fractions by Atmospheric Pressure Laser Ionization Fourier Transform Ion Cyclotron Resonance Mass Spectrometry. *Energy & Fuels* **2012,** *26* (6), 3481-3487.
6. Boduszynski, M. M.; Hurtubise, R. J.; Allen, T. W.; Silver, H. F., Liquid-Chromatography Field-Ionization Mass-Spectrometry in the Analysis of High-Boiling and Nondistillable Coal Liquids for Hydrocarbons. *Analytical Chemistry* **1983,** *55* (2), 225-231.

7. Chapter 5 Silica columns–packing procedures and performance characteristics. In *Journal of Chromatography Library*, Unger, K. K., Ed. Elsevier: 1979; Vol. 16, pp 169-186.
8. Bickler, B. So, what exactly is a column volume in flash column chromatography and how is it determined? https://selekt.biotage.com/blog/so-what-exactly-is-a-column-volume-in-flash-column-chromatography-and-how-is-it-determined (accessed July 17, 2020).
9. Nebbioso, A.; Piccolo, A., Molecular characterization of dissolved organic matter (DOM): a critical review. *Analytical and Bioanalytical Chemistry* **2013,** *405* (1), 109-124.
10. Killops, S.; Killops, V., *An Introduction to Organic Geochemistry*. 2005; p 393.
11. Griffith, D.; McNichol, A.; Xu, L.; McLaughlin, F.; Macdonald, R.; Brown, K.; Eglinton, T., Carbon dynamics in the western Arctic Ocean: Insights from full-depth carbon isotope profiles of DIC, DOC, and POC. *Biogeosciences* **2012,** *9*, 1217-1224.
12. Hatakka, A., Biodegradation of Lignin. In *Biopolymers Online*.
13. Lønborg, C.; Carreira, C.; Jickells, T.; Álvarez-Salgado, X. A., Impacts of Global Change on Ocean Dissolved Organic Carbon (DOC) Cycling. *Frontiers in Marine Science* **2020,** *7*, 466.
14. National Research Council Committee on Oil in the Sea: Inputs, F.; Effects, In *Oil in the Sea III: Inputs, Fates, and Effects*, National Academies Press (US) Copyright 2003 by the National Academy of Sciences. All rights reserved.: Washington (DC), 2003.
15. Wilde, M. J.; Rowland, S. J., Structural Identification of Petroleum Acids by Conversion to Hydrocarbons and Multidimensional Gas Chromatography-Mass Spectrometry. *Analytical Chemistry* **2015,** *87* (16), 8457-8465.
16. Tarr, M.; Zito, P.; Overton, E.; Olson, G.; Adkikari, P.; Reddy, C., Weathering of Oil Spilled in the Marine Environment. *Oceanography* **2016,** *29* (3), 126-135.
17. Wilson, W. B.; Hayes, H. V.; Sander, L. C.; Campiglia, A. D.; Wise, S. A., Normal-phase liquid chromatography retention behavior of polycyclic aromatic hydrocarbon and their methyl-substituted derivatives on an aminopropyl stationary phase. *Analytical and Bioanalytical Chemistry* **2017,** *409* (22), 5291-5305.
18. Zito, P.; Podgorski, D. C.; Johnson, J.; Chen, H.; Rodgers, R. P.; Guillemette, F.; Kellerman, A. M.; Spencer, R. G. M.; Tarr, M. A., Molecular-Level Composition and Acute Toxicity of Photosolubilized Petrogenic Carbon. *Environmental Science & Technology* **2019,** *53* (14), 8235-8243.
19. Wagner, S.; Jaffé, R., Effect of photodegradation on molecular size distribution and quality of dissolved black carbon. *Organic Geochemistry* **2015,** *86*, 1-4.
20. Speight, J. G., *Handbook of Petroleum Analysis. Chemical Analysis: A series of Monographs on Analytical Chemistry and its Applications*. Wiley Interscience: New York, 2001; Vol. 158, p 1.
21. Mckenna, A. M. Detailed Characterization of Heavy Crude Oils and Asphaltenes by Ultrahigh Resolution Fourier Transform Ion Cyclotron Resonance Mass Spectrometry. Dissertation, Florida State University, Tallahassee, 2009.
22. Akbarzadeh, K.; Hammami, A.; Kharrat, A.; Zhang, D.; Allenson, S.; Creek, J.; Kabir, S.; Jamaluddin, A.; Marshall, A. G.; Rodgers, R.; Mullins, O.; Solbakken, T., Asphaltenes - problematic but rich in potential. *Oilfield Review* **2007,** *19*, 22-43.
23. Mullins, O., Review of the Molecular Structure and Aggregation of Asphaltenes and Petroleomics. *SPE Journal - SPE J* **2008,** *13*, 48-57.

24. Podgorski, D. C.; Corilo, Y. E.; Nyadong, L.; Lobodin, V. V.; Bythell, B. J.; Robbins, W. K.; McKenna, A. M.; Marshall, A. G.; Rodgers, R. P., Heavy Petroleum Composition. 5. Compositional and Structural Continuum of Petroleum Revealed. *Energy & Fuels* **2013,** *27* (3), 1268-1276.
25. Podgorski, D. C.; Zito, P.; Kellerman, A. M.; Bekins, B. A.; Cozzarelli, I. M.; Smith, D. F.; Cao, X.; Schmidt-Rohr, K.; Wagner, S.; Stubbins, A.; Spencer, R. G. M., Hydrocarbons to carboxyl-rich alicyclic molecules: A continuum model to describe biodegradation of petroleum-derived dissolved organic matter in contaminated groundwater plumes. *Journal of Hazardous Materials* **2021,** *402*, 123998.
26. Cho, Y.; Na, J.-G.; Nho, N.-S.; Kim, S.; Kim, S., Application of Saturates, Aromatics, Resins, and Asphaltenes Crude Oil Fractionation for Detailed Chemical Characterization of Heavy Crude Oils by Fourier Transform Ion Cyclotron Resonance Mass Spectrometry Equipped with Atmospheric Pressure Photoionization. *Energy & Fuels* **2012,** *26* (5), 2558-2565.
27. Sillanpää, M.; Matilainen, A.; Lahtinen, T., Chapter 2 - Characterization of NOM. In *Natural Organic Matter in Water*, Sillanpää, M., Ed. Butterworth-Heinemann: 2015; pp 17-53.
28. Boduszynski, M. M.; Hurtubise, R. J.; Allen, T. W.; Silver, H. F., Liquid chromatography/field ionization mass spectrometry in the analysis of high-boiling and nondistillable coal liquids for hydrocarbons. *Analytical Chemistry* **1983,** *55* (2), 225-231.
29. Boduszynski, M. M.; Altgelt, K. H., Composition of heavy petroleums. 4. Significance of the extended atmospheric equivalent boiling point (AEBP) scale. *Energy & Fuels* **1992,** *6* (1), 72-76.
30. Boduszynski, M. M., Composition of heavy petroleums. 1. Molecular weight, hydrogen deficiency, and heteroatom concentration as a function of atmospheric equivalent boiling point up to 1400.degree.F (760.degree.C). *Energy & Fuels* **1987,** *1* (1), 2-11.
31. Boduszynski, M. M., Composition of heavy petroleums. 2. Molecular characterization. *Energy & Fuels* **1988,** *2* (5), 597-613.
32. Farmani, Z.; Schrader, W., A Detailed Look at the Saturate Fractions of Different Crude Oils Using Direct Analysis by Ultrahigh Resolution Mass Spectrometry (UHRMS). *Energies* **2019,** *12*, 3455.
33. Bastow, T. P.; van Aarssen, B. G. K.; Lang, D., Rapid small-scale separation of saturate, aromatic and polar components in petroleum. *Organic Geochemistry* **2007,** *38* (8), 1235-1250.
34. Islasflores, C.; Buenrostrogonzalez, E.; Liragaleana, C., Fractionation of petroleum resins by normal and reverse phase liquid chromatography. *Fuel* **2006,** *85* (12-13), 1842-1850.
35. Putman, J. C.; Rowland, S. M.; Podgorski, D. C.; Robbins, W. K.; Rodgers, R. P., Dual-Column Aromatic Ring Class Separation with Improved Universal Detection across Mobile-Phase Gradients via Eluate Dilution. *Energy & Fuels* **2017,** *31* (11), 12064-12071.
36. Nomura, A.; Yamada, J.; Tsunoda, K.-i., Acylation of Aminopropyl-Bonded Silica Gel for Liquid Chromatography. *Analytical Sciences* **1987,** *3* (3), 209-212.
37. Wise, S. A.; Chesler, S. N.; Hertz, H. S.; Hilpert, L. R.; May, W. E., Chemically-bonded aminosilane stationary phase for the high-performance liquid chromatographic separation of polynuclear aromatic compounds. *Analytical Chemistry* **1977,** *49* (14), 2306-2310.
38. Cory, R. M.; Kling, G. W., Interactions between sunlight and microorganisms influence dissolved organic matter degradation along the aquatic continuum. *Limnology and Oceanography Letters* **2018,** *3* (3), 102-116.
39. Zito, P.; Podgorski, D. C.; Bartges, T.; Guillemette, F.; Roebuck, J. A.; Spencer, R. G. M.; Rodgers, R. P.; Tarr, M. A., Sunlight-Induced Molecular Progression of Oil into Oxidized

Oil Soluble Species, Interfacial Material, and Dissolved Organic Matter. *Energy & Fuels* **2020,** *34* (4), 4721-4726.
40. Bacosa, H. P.; Erdner, D. L.; Liu, Z., Differentiating the roles of photooxidation and biodegradation in the weathering of Light Louisiana Sweet crude oil in surface water from the Deepwater Horizon site. *Mar Pollut Bull* **2015,** *95* (1), 265-72.
41. Harriman, B. H.; Zito, P.; Podgorski, D. C.; Tarr, M. A.; Suflita, J. M., Impact of Photooxidation and Biodegradation on the Fate of Oil Spilled During the Deepwater Horizon Incident: Advanced Stages of Weathering. *Environ Sci Technol* **2017,** *51* (13), 7412-7421.
42. Fellman, J. B.; Hood, E.; Spencer, R. G. M., Fluorescence spectroscopy opens new windows into dissolved organic matter dynamics in freshwater ecosystems: A review. *Limnology and Oceanography* **2010,** *55* (6), 2452-2462.
43. Wunsch, U. J.; Murphy, K. R.; Stedmon, C. A., The One-Sample PARAFAC Approach Reveals Molecular Size Distributions of Fluorescent Components in Dissolved Organic Matter. *Environ Sci Technol* **2017,** *51* (20), 11900-11908.
44. Murphy, K. R.; Stedmon, C. A.; Graeber, D.; Bro, R., Fluorescence spectroscopy and multi-way techniques. PARAFAC. *Analytical Methods* **2013,** *5* (23), 6557-6566.
45. Bro, R.; Kiers, H. A. L., A new efficient method for determining the number of components in PARAFAC models. *Journal of Chemometrics* **2003,** *17* (5), 274-286.
46. Ohno, T., Fluorescence inner-filtering correction for determining the humification index of dissolved organic matter. *Environ Sci Technol* **2002,** *36* (4), 742-6.
47. Kowalczuk, P.; Cooper, W.; Whitehead, R.; Durako, M.; Sheldon, W., Characterization of CDOM in an organic-rich river and surrounding coastal ocean in the South Atlantic Bight. *Aquatic Sciences* **2003,** *65*, 384-401.
48. Stedmon, C. A.; Bro, R., Characterizing dissolved organic matter fluorescence with parallel factor analysis: a tutorial. *Limnology and Oceanography: Methods* **2008,** *6* (11), 572-579.
49. Hansen, A. M.; Kraus, T. E. C.; Pellerin, B. A.; Fleck, J. A.; Downing, B. D.; Bergamaschi, B. A., Optical properties of dissolved organic matter (DOM): Effects of biological and photolytic degradation. *limnology and oceanography* **2016,** *61* (3), 1015-1032.
50. Weishaar, J. L.; Aiken, G. R.; Bergamaschi, B. A.; Fram, M. S.; Fujii, R.; Mopper, K., Evaluation of specific ultraviolet absorbance as an indicator of the chemical composition and reactivity of dissolved organic carbon. *Environ Sci Technol* **2003,** *37* (20), 4702-8.
51. Yamashita, Y.; Boyer, J. N.; Jaffé, R., Evaluating the distribution of terrestrial dissolved organic matter in a complex coastal ecosystem using fluorescence spectroscopy. *Continental Shelf Research* **2013,** *66*, 136-144.
52. Podgorski, D. C.; Zito, P.; McGuire, J. T.; Martinovic-Weigelt, D.; Cozzarelli, I. M.; Bekins, B. A.; Spencer, R. G. M., Examining Natural Attenuation and Acute Toxicity of Petroleum-Derived Dissolved Organic Matter with Optical Spectroscopy. *Environmental Science & Technology* **2018,** *52* (11), 6157-6166.
53. Derrien, M.; Shin, K.-H.; Hur, J., Assessment on applicability of common source tracking tools for particulate organic matter in controlled end member mixing experiments. *Science of The Total Environment* **2019,** *666*, 187-196.
54. Brym, A.; Paerl, H. W.; Montgomery, M. T.; Handsel, L. T.; Ziervogel, K.; Osburn, C. L., Optical and chemical characterization of base-extracted particulate organic matter in coastal marine environments. *Marine Chemistry* **2014,** *162*, 96-113.

55. Zhou, Y.; Martin, P.; Müller, M., Composition and cycling of dissolved organic matter from tropical peatlands of coastal Sarawak, Borneo, revealed by fluorescence spectroscopy and parallel factor analysis. *Biogeosciences* **2019,** *16*, 2733.
56. Dainard, P. G.; Guéguen, C.; McDonald, N.; Williams, W. J., Photobleaching of fluorescent dissolved organic matter in Beaufort Sea and North Atlantic Subtropical Gyre. *Marine Chemistry* **2015,** *177*, 630-637.

Appendix

File list for exported corrected EEMS in Figure 12.

1	1-2R 96hrSEM.dat'
2	5+ 0hrSEM.dat'
3	5+ 24hrSEM.dat'
4	3-4R 0hrSEM.dat'
5	5+ 48hrSEM.dat'
6	5+ 72 hrSEM.dat'
7	5+ 96hrSEM.dat'
8	Sat 0hrSEM.dat'
9	3-4R 24hrSEM.dat'
10	Sat 24hrSEM.dat'
11	3-4R 48hrSEM.dat'
12	Sat 48hrSEM.dat'
13	3-4R 72hrSEM.dat'
14	Sat 72hrSEM.dat'
15	3-4R 96hrSEM.dat'
16	Sat 96hrSEM.dat'
17	1-2R 0hrSEM.dat'
18	1-2R 24hrSEM.dat'
19	1-2R 48hrSEM.dat'
20	1-2R 72hrSEM.dat'

VITA

The author was born in Greer, South Carolina. He obtained his bachelor's degree in chemistry from the University of New Orleans in 2017. He joined the University of New Orleans chemistry graduate program to pursue a master's based thesis in analytical chemistry, and became a member of Dr. Phoebe Zito and Dr. David Podgorski's research groups in 2018.